IEEE Access
Multidisciplinary ⋮ Rapid Review ⋮ Open Access Journal

Received March 28, 2022, accepted May 18, 2022, date of publication May 23, 2022, date of current version May 27, 2022.

Digital Object Identifier 10.1109/ACCESS.2022.3177192

Novel Transformerless Multilevel Inductive Power Transfer System

JAEHONG LEE[1], (Graduate Student Member, IEEE), MYUNG-YONG KIM[2], (Member, IEEE), AND SEUNG-HWAN LEE[1], (Member, IEEE)

[1]School of Electrical and Computer Engineering, University of Seoul, Seoul 02504, South Korea
[2]Smart Electrical and Signaling Division, Korea Railroad Research Institute, Uiwang 16105, South Korea

Corresponding author: Seung-Hwan Lee (seunghlee16@uos.ac.kr)

This work was supported by the National Research Foundation of Korea (NRF) funded by the Korea Government [Ministry of Science and ICT (MSIT)] under Grant 2021R1A2C2009335.

ABSTRACT Previous high power on-line inductive power transfer (IPT) systems use line-frequency (LF) transformers and high-frequency (HF) transformers to be compatible with the ratings of commercial power switches. However, LF and HF transformers make the IPT systems bulky and expensive. This study proposes a new transformerless multilevel on-line IPT system using multilevel rectifiers, inverters, and excitation coils. Instead of the LF transformers, a series-connected multilevel rectifier and inverter are used. Instead of the HF transformers, excitation coils, which have strong magnetic couplings with a transmitter coil, is connected to each of the output terminals of the multilevel inverter. The magnetic fields generated by the multiple excitation coils induce a high voltage and current in the transmitter coil. The induced current generates the augmented magnetic field in the transmitter; therefore, a receiver coil that is loosely coupled with the transmitter can collect power from the mains. The input impedance, voltage and current gains, and efficiency of the proposed IPT system are investigated using an equivalent circuit model. The impact of the excitation coil shape on the magnetic couplings is explored using finite element analysis. Based on the investigation, a design for the excitation coil is presented. The feasibility of the proposed system is evaluated using a 4-level experimental test-bed. Measured coil-to-coil and DC-to-load efficiencies of the proposed system are observed to be 88% and 84%, respectively, over a 7 cm air-gap.

INDEX TERMS Excitation coil, impedance matching, inductive power transfer, wireless power transfer, multilevel converter.

I. INTRODUCTION

IPT systems can deliver power from energy sources to loads without any physical contact [1]–[4]. Because they are more convenient, safe, and reliable than conventional power supplies, many researchers have developed stationary or in-motion IPT systems for electric cars, buses, and trains [5]–[9].

Fig. 1 shows a block diagram of a high power on-line IPT system in [9]. Line-frequency (LF) transformers are used at the front end of the IPT system to make the medium-voltage (MV) input down to 750 V_{DC}, a reliable level for commercially available power semiconductors. Parallel-connected H-bridge inverters are connected to the rectifier's DC bus to expand the power level. The output voltages of the inverters are connected to primary windings of high-frequency (HF) transformers, which have series-connected secondary windings. The output powers of the inverters are aggregated by the transformers' series- connected secondary windings, which are supplying a net voltage of 3 kV_{rms} to the transmitter coil. It should be noted that this study uses the LF and HF transformers to build the MV system. The structure of this IPT system is straightforward and easy to implement. However, the power density and cost-effectiveness of the IPT system are not good because it requires bulky transformers.

Li *et al.* proposed a multilevel IPT system with active rectifiers and cascaded H-bridge inverters to eliminate the LF transformer [10]. In this study, a transmitter coil and a compensation capacitor are connected in series with the multilevel inverter. This topology is conducive to supplying high voltage output to the transmitter coil at high switching frequencies. However, high-voltage insulations of the transmitter coil and

The associate editor coordinating the review of this manuscript and approving it for publication was Snehal Gawande.

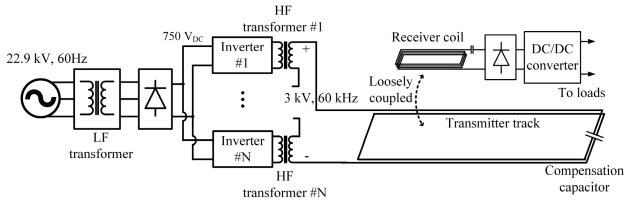

FIGURE 1. Block diagram of an on-line IPT system with LF and HF transformers.

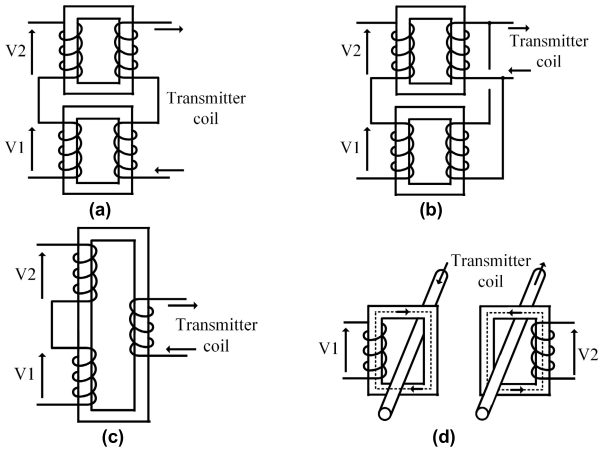

FIGURE 2. Four magnetic configurations of multilevel system. (a) HF transformers with series-connected secondary windings. (b) HF transformers with parallel-connected secondary windings. (c) Multi-windings HF transformer. (d) Proposed excitation and transmitter coils.

the resonant-tuning capacitors are drawbacks of this system. It is very challenging to apply the proposed idea to the MV system.

Park *et al.* proposed a multilevel inverter with HF transformers with secondary windings connected in series like Fig. 2(a) [11]. However, the high voltage insulation between the primary windings and the cores of the HF transformer makes the system bulky and expensive. In addition, a failure of one winding of the transformers results shutdown of the entire system. Ayyanar *et al.* used HF transformers with parallel-connected secondary windings at the outputs of the multilevel inverter as Fig. 2(b) [12]. It should be noted that the parallel-connected secondary windings can suffer from a large circulation current because of the voltage imbalance between the transformers. HF transformers that have two or more primary windings with a single secondary winding can be employed for the multilevel system as Fig. 2(c) [13]–[15]. Augmented magnetic fields of the primary windings can induce high voltage and current at the secondary winding terminal. However, it is required to replace the entire transformer even for a failure of a single winding of the primary side.

A new multilevel IPT system was proposed in [16], which uses multiple excitation coils (see Fig. 2(d)) instead of the HF transformers. Like the multiple primary winding HF transformer, synchronized magnetic fields generated by the excitation coils are augmented and induced high voltage and

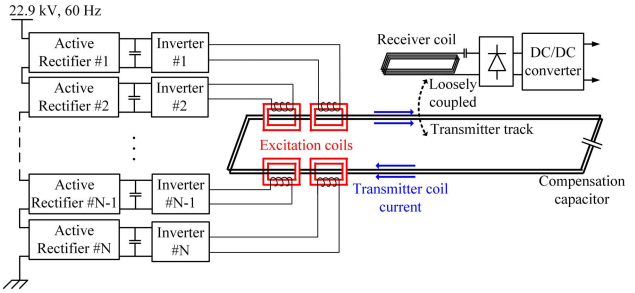

FIGURE 3. Proposed multilevel IPT system with excitation coils.

current to the transmitter coil. Then, the magnetic field generated by the current of the transmitter coil induces voltage and current to the receiver coil, which is loosely coupled with the transmitter coil. The excitation coils are galvanically isolated and have strong magnetic couplings with the transmitter coil. However, the excitation coils do not have couplings with the other excitation coils. This is the unique feature of the study. Because the excitation coils are isolated to each other, this system has the following four advantages compared to the conventional multilevel IPT systems: 1) ease of modularization, 2) fail-safe operation, 3) ease of high voltage insulation, and 4) high power density. Since the excitation coils have no magnetic coupling between them, the excitation coil and its driving inverter can be easily modularized without interfering with other excitation coils and inverters. In addition, a failure of one excitation coil results in a $1/N$ reduction of the induced voltage at the transmitter and the receiver coil (N is the total number of excitation coils). Therefore, the failure of a few excitation coils or a few converters does not significantly affect the performance of the proposed IPT system. Furthermore, because there are large air gaps between the transmitter coil and the excitation coils, the high voltage insulation of the excitation coil can be easily implemented. Finally, because the power level of each excitation coil is very small compared to the total output power, the excitation coil can be implemented in a compact volume. An overall configuration of the proposed multilevel on-line IPT system is shown in Fig. 3. The IPT system includes a multilevel active rectifier, a multilevel inverter, excitation coils, a transmitter coil, a receiver coil, a receiver rectifier, a receiver-side DC/DC converter, and a load. This paper expands the discussion in [16] by including additional circuit analysis on the resonant frequencies and the current and voltage gains of multi-coil IPT system. Also, this study includes the impact of excitation coil shape on magnetic couplings and self-inductances of the coils. Based on the analysis, a design for the excitation coil is proposed as well. In addition, a 4-level IPT system is built to evaluate the proposed configuration experimentally. In the first part of this paper, the proposed multilevel on-line IPT system with excitation coils is demonstrated and analyzed using a T-type equivalent circuit model. In the following section, an excitation coil design is demonstrated using theoretical and finite element analysis (FEA) results. In the last section, the viability of the proposed IPT system is evaluated using experimental results.

II. ANALYSIS OF PROPOSED MULTILEVEL IPT SYSTEM

Fig. 4 shows an equivalent circuit model of the proposed multilevel IPT system with N excitation coils. The series-connected voltage sources represent series-connected rectifiers and inverters at the front end. An inductor L_m and a capacitor C_m are included to transform the input impedance at low- and high-frequency ranges. L_{ex} is the self-inductance of the excitation coil, and L_{tx} and C_{tx} are the self-inductance and capacitance of the transmitter resonant tank, respectively. L_{rx} and C_{rx} are the self-inductance and capacitance of the receiver resonant tank, respectively. R_{ex},R_{tx}, and R_{rx} are the equivalent-series-resistances (ESRs) of the excitation, transmitter, and receiver coils, respectively. k_{extx} is the coupling coefficient between the excitation coil and transmitter coil, and the k_{txrx} is the coupling coefficient between the transmitter and receiver coils. I_{txN} and I_{rxN} are currents of the transmitter and receiver coils induced by N excitation coils, respectively.

Fig. 5 shows an equivalent circuit model seen from one of the excitation coils. $M_{extx} = k_{extx}\sqrt{L_{ex}L_{tx}}$ is the mutual-inductance between the excitation and transmitter coils and $M_{txrx} = k_{txrx}\sqrt{L_{tx}L_{rx}}$ is the mutual-inductance between the transmitter and receiver coils. $I_{tx} = I_{txN}/N$ and $I_{rx} = I_{rxN}/N$ are the transmitter and receiver coil currents induced by one of the N excitation coils, respectively. To find the input impedance seen from one of the excitation coils, the inductances and resistances in the transmitter and receiver circuits are multiplied by N, and the capacitances are divided by N.

A. INPUT IMPEDANCE SEEN FROM A SINGLE EXCITATION COIL

Using the equivalent circuit in Fig. 5, the input impedance seen from one of the excitation coils follows (1).

$$Z_{in} = Z_{ex} - j\omega M_{extx}N + Z_{cmb}N \tag{1}$$

where, ω is the angular operating frequency, $Z_{ex} = j\omega L_{ex} + j\omega L_m + 1/(j\omega C_m) + R_{ex}$ is the impedance of the excitation resonant tank, $Z_{tx} = j\omega L_{tx} + 1/(j\omega C_{tx}) + R_{tx}$ is the impedance of the transmitter resonant tank, $Z_{rx} = j\omega L_{rx} + 1/(j\omega C_{rx}) + R_{rx} + R_L$ is the impedance of the receiver resonant tank, and $Z_{cmb} = j\omega M_{extx}(Z_{tx}Z_{rx} + \omega^2 M_{txrx}^2 - j\omega M_{extx}Z_{rx})/(Z_{tx}Z_{rx} + \omega^2 M_{txrx}^2)$ is the impedance of the combined circuit of the transmitter and receiver resonant tanks (see Fig. 5). N is the number of excitation coils.

Using (1) and selected circuit parameters in TABLE 1, frequency responses of Z_{in} with different numbers of excitation coils are plotted in Fig. 6. It should be noted that the impedance plot has three resonant frequencies. The first resonant frequency f_{r1}, which is caused by the series resonance between $L_m + L_{ex}$ and C_m, follows (2).

$$f_{r1} = \frac{1}{2\pi\sqrt{(L_m + L_{ex})\,C_m}} \tag{2}$$

Parameter robustness of the multiple excitation coil system depends on the f_{r1} as parameter errors exist on the L_m, L_{ex}, and C_m. Furthermore, parameter mismatches can generate

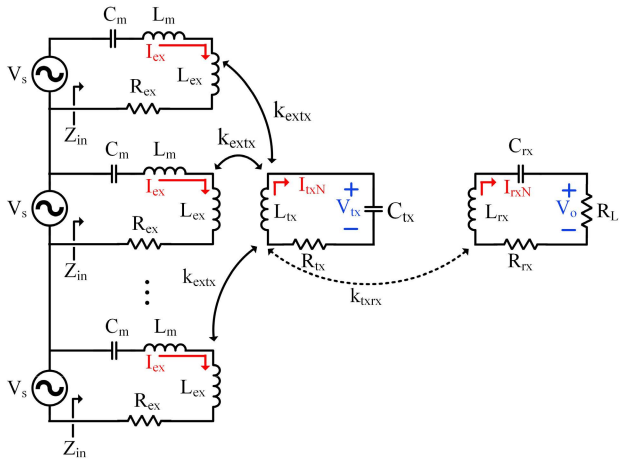

FIGURE 4. Equivalent circuit model of the IPT system with multiple excitation coils.

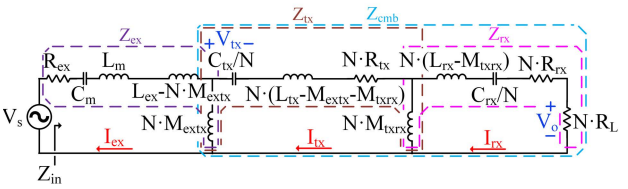

FIGURE 5. T-equivalent circuit model of the multiple excitation coil system.

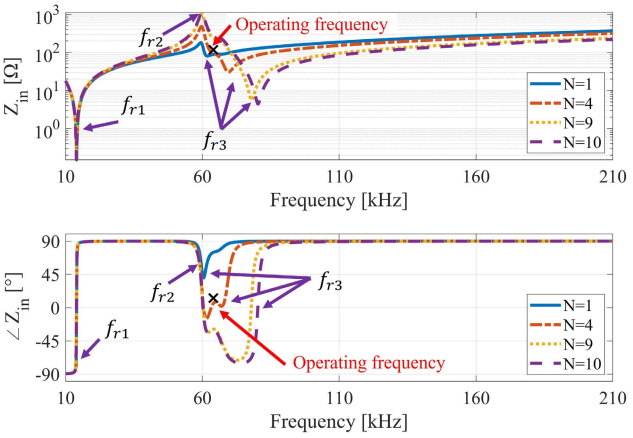

FIGURE 6. Input impedance seen from one of the excitation coils of the proposed multilevel IPT system.

additional resonances by combining with other resonant tanks (transmitter and receiver). Fig. 7(a) shows the frequency responses of Z_{in} seen from excitation coils of a 4-level IPT system when f_{r1} is 60 kHz (very close to the tuning frequencies of the transmitter and the receiver). The matching inductance of the second level L_m' has a 10% error compared to the other levels' matching inductances. It should be noted that the 10% error in L_m significantly distorts the input impedances at the tuning frequencies of the coils. Fig. 7(b) shows the frequency responses of Z_{in} seen from excitation coils of a 4-level IPT system when f_{r1} is 15 kHz. The impact

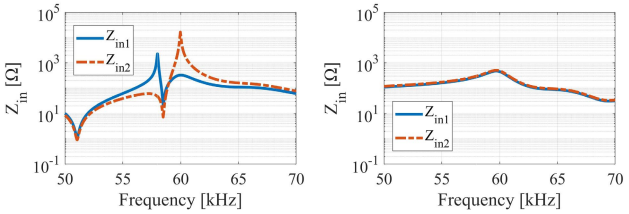

FIGURE 7. Input impedance with 10% parameter errors on L_m. (a) $f_{r1} = 60$ kHz. (b) $f_{r1} = 15$kHz .

TABLE 1. Selected circuit parameters for proposed IPT system.

Parameters of excitation resonance tank			
L_m	200 μH	L_{ex}	90 μH
C_m	440 nF	R_{ex}	150 mΩ
Parameters of transmitter resonance tank			
L_{tx}	8.5 μH	R_{tx}	20 mΩ
C_{tx}	795 nF		
Parameters of receiver resonance tank			
L_{rx}	17.3 μH	R_{rx}	45 mΩ
C_{rx}	352 nF	R_L	0.8 Ω
Coupling coefficients between coils			
k_{extx}	0.35	k_{txrx}	0.1

of parameter error is decreased significantly compared to the previous case. Therefore, the tuning frequency f_{r1} is selected to be 15 kHz to avoid the effects of parameter errors of L_{ex}, L_m, and C_m. This is much lower than the tuned frequencies of the transmitter and receiver coils (61 kHz and 64 kHz, respectively).

The second resonant frequency f_{r2} is caused by the parallel resonance between the transmitter and receiver tanks. The f_{r2} is the frequency that satisfies a condition (3) and an approximated solution of f_{r2} is shown in (4).

$$Re\left(Z_{tx}Z_{rx}\right) - \left(\omega M_{txrx}\right)^2 = 0 \tag{3}$$

$$f_{r2} \approx \begin{cases} \dfrac{f_{tx}}{\sqrt{1-k_{txrx}^2}} & if f_{tx} < f_{rx} \\ \dfrac{f_{rx}}{\sqrt{1-k_{txrx}^2}} & if f_{tx} > f_{rx} \end{cases} \tag{4}$$

where $Re()$ is an operator that denotes the real part of a complex number, and $f_{tx} = 1/(2\pi\sqrt{L_{tx}C_{tx}})$ and $f_{rx} = 1/(2\pi\sqrt{L_{rx}C_{rx}})$ are the tuning frequencies of the transmitter and receiver coils, respectively. It should be noted that the peak magnitude of Z_{in} at f_{r2} increases with the increase of N as shown in Fig. 6. Therefore, f_{r2} is not a suitable operating frequency for a multilevel system with the large number of N.

The third resonant frequency f_{r3} is caused by the combined resonance between the excitation, transmitter, and receiver coils. This frequency satisfies the condition (5).

$$Im\left(Z_{ex}Z_{tx}Z_{rx} + Z_{ex}\left(\omega M_{txrx}\right)^2 + Z_{rx}\left(\omega M_{extx}\right)^2 N\right) = 0 \tag{5}$$

where $Im()$ is an operator that denotes the imaginary part of a complex number. Because of its complexity, its closed form solution is shown in Appendix. Unlike the resonant frequencies f_{r1} and f_{r2}, the frequency f_{r3} moves away as the number of N increases, resulting in magnitude and phase variations of the input impedance.

B. CURRENT AND VOLTAGE AMPLIFICATIONS

The current gain of the transmitter coil to the excitation coil with N excitation coils can be calculated as (6).

$$G_i = \frac{I_{txN}}{I_{ex}} = \left|\frac{j\omega M_{extx}Z_{rx}N}{Z_{tx}Z_{rx} + \left(\omega M_{txrx}\right)^2}\right| \tag{6}$$

Fig. 8(a) shows a frequency response of the current gain with different numbers of excitation coils. The current gain is amplified by a factor of N with multiple excitation coils.

From Figs. 4 and 5, the gain of the transmitter voltage V_{tx} to the input voltage V_s, and the gain of the output voltage V_o to the transmitter voltage V_{tx} with N excitation coils are calculated as (7) and (8).

$$G_{v\_extx} = \frac{V_{tx}}{V_s} = \left|\frac{M_{extx}Z_{rx}N/C_{tx}}{Z_{ex}Z_{tx}Z_{rx} + Z_{ex}\left(\omega M_{txrx}\right)^2 + Z_{rx}\left(\omega M_{extx}\right)^2 N}\right| \tag{7}$$

$$G_{v\_txrx} = \frac{V_o}{V_{tx}} = \left|\frac{j\omega^2 C_{tx}M_{txrx}R_L}{Z_{rx}}\right| \tag{8}$$

Fig. 8(b) shows a frequency response of the voltage gain of V_{tx}/V_s with different numbers of excitation coils. Unlike the current gain, the maximum voltage gain appears at f_{r3}. Fig. 8(c) shows frequency responses of the voltage gain of V_o/V_{tx} with different numbers of excitation coils. It should be noted that the voltage gain is independent on the number of excitation coils. Fig. 8(d) shows frequency responses of the voltage gain of V_o/V_s. Like the responses of V_{tx}/V_s, the frequency response of V_o/V_s has its peak at f_{r3}.

C. EFFICIENCY

The coil-to-coil efficiency of the IPT system with N excitation coils follows (9).

$$\eta = \frac{I_{rxN}^2 R_L}{I_{ex}^2 R_{ex}N + I_{txN}^2 R_{tx} + I_{rxN}^2\left(R_{rx} + R_L\right)} \tag{9}$$

The I_{ex}, I_{txN}, and I_{rxN} are shown in Fig. 4. Fig. 9 shows the calculated coil-to-coil efficiency using (9). The peak efficiency appears at the tuned frequency of the receiver coil and is insensitive to the number of excitation coils. In this study, the tuned frequency of the receiver coil is selected as the operating frequency to have maximum efficiency at the rated load. As the number of excitation coils increases, the losses of the excitation coils are negligible compared to other losses. The loss of the excitation coil is proportional to N, while the losses of the transmitter and receiver coils increase by a factor of N^2.

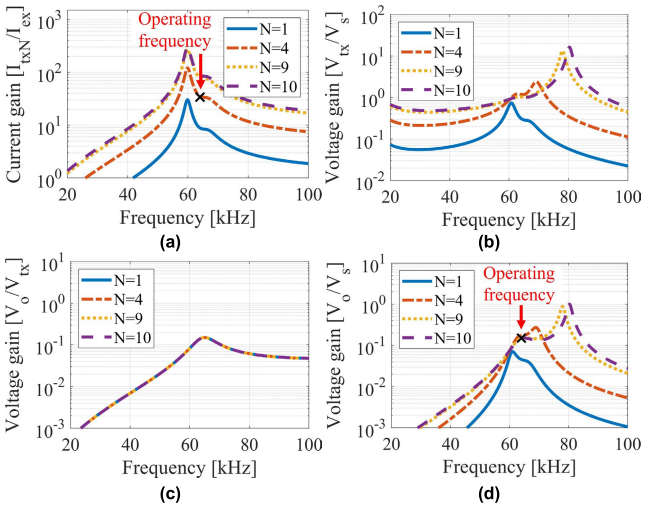

FIGURE 8. Current and voltage gains of the IPT system with multiple excitation coils. (a) Current gain of the transmitter coil current to the excitation coil current. (b) Voltage gain of the transmitter voltage to the input voltage. (c) Voltage gain of the output voltage to the transmitter voltage. (d) Voltage gain of the output voltage to the input voltage.

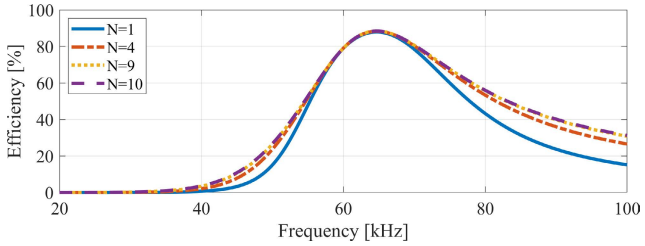

FIGURE 9. Theoretical coil-to-coil efficiency of the IPT system with multiple excitation coils.

III. EXCITATION COIL DESIGN

To implement the proposed multilevel IPT system, practical design for the excitation coil is required. A new design for the excitation coil for the proposed IPT system is demonstrated in this section.

A. TRANSMITTER AND RECEIVER COILS

The transmitter is single-turn (two wires in parallel), coreless, 2 m long, 20 cm wide, and 2 cm turn spacing. The receiver coil is four-turn, ferrite-cored, 50 cm long, 30 cm wide, and 2 cm turn spacing. The lengths of the transmitter and receiver coils are 2 m and 50 cm, respectively, for a laboratory test. The air gap between the transmitter and receiver coils is 7 cm. Fig. 10(a) and (b) show the transmitter and receiver coils, respectively.

B. PROPOSED EXCITATION COIL DESIGN

As mentioned earlier, the excitation coil needs a strong coupling with the transmitter coil but very weak couplings with other coils. Fig. 11 shows the design of the proposed excitation coil. Four ferrite plates form a hollow hexahedron, which wraps around the transmitter coil. The excitation coil is wound around the bottom plate in a parallel direction to the transmitter coil. The magnetic field generated by the

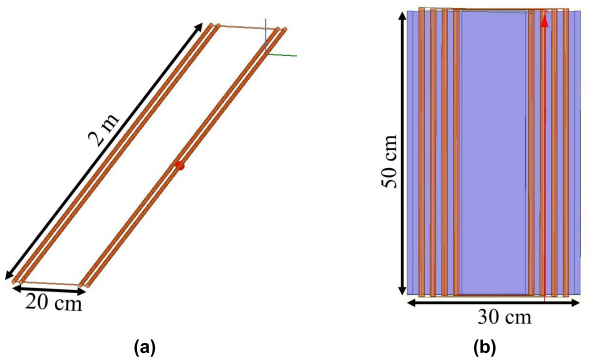

FIGURE 10. Details of the coils. (a) Transmitter coil. (b) Receiver coil.

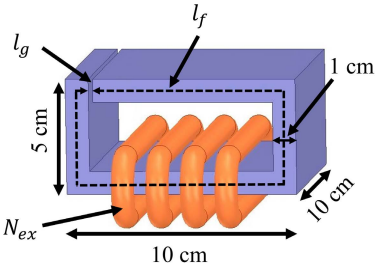

FIGURE 11. Proposed excitation coil.

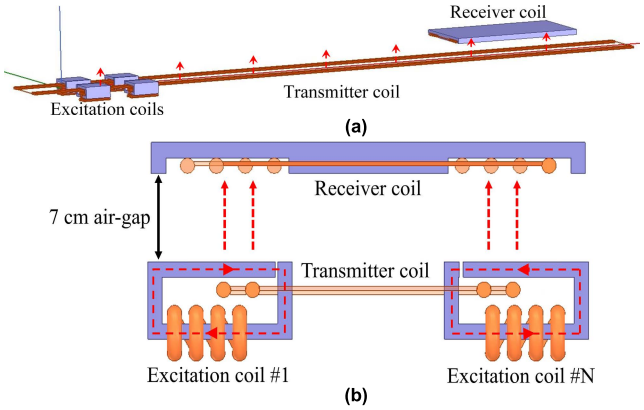

FIGURE 12. Configuration of the proposed multilevel IPT system. (a) Side view. (b) Front view.

excitation coil flows through the ferrite core and couples with the transmitter coil. Since the ferrite core can efficiently confine the magnetic field inside the core, the proposed design has a strong magnetic coupling with the transmitter coil and a weak coupling with the receiver coil.

As it is shown in Fig. 11, the mean path length (MPL) l_f, air-gap length l_g, cross-sectional area of the core S, and the number of turns of the coil N_{ex} are the design parameters to achieve the required self-inductance and the coupling coefficients in TABLE 1. For the core, ferrite cores that are made with PL11 (Samwha electronics) [17]. The sizes of the ferrite cores that are used in the design are 1 cm × 10 cm × 10 cm and 1 cm × 4 cm × 10 cm. Because the permeability of the PL11 core (initial permeability = 2500) is much larger than that of air, the reluctance of the air is a dominant factor for the inductance and coupling. Therefore, the MPL l_f is not

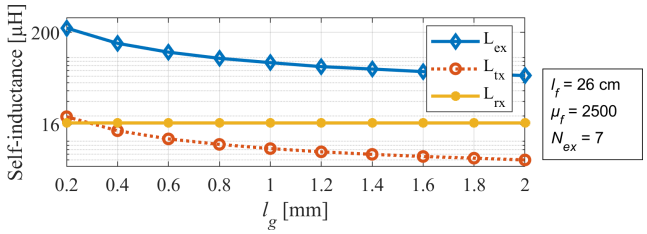

FIGURE 13. FEA results of self-inductances of the excitation, transmitter, and receiver coils with l_g.

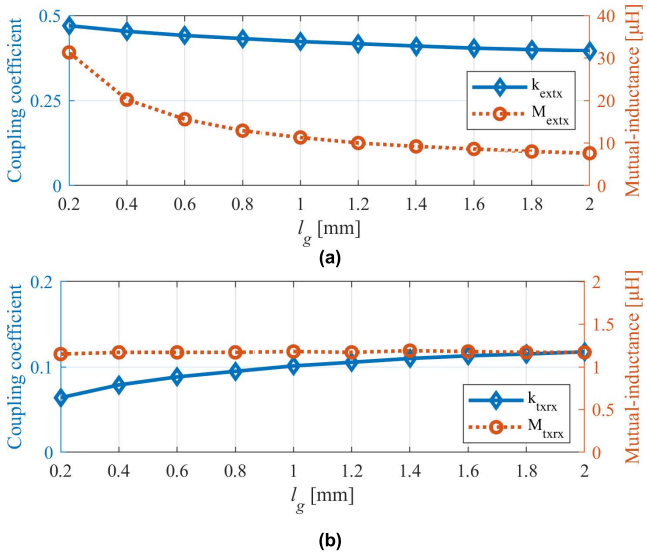

FIGURE 14. FEA results of coupling coefficients and mutual-inductances with l_g. (a) Between excitation and transmitter coils. (b) Between transmitter and receiver coils.

a critical parameter in the excitation coil design. The l_f is selected to be 26 cm to ensure sufficient distance from the transmitter coil. The air gap l_g is the critical parameter that are investigated in this study. Using an FEA simulation software, ANSYS HFSS [18], the dependence of the self- and mutual-inductances of the transmitter, receiver, and excitation coils on the opening l_g are investigated. Fig. 12 shows details of the simulation model. The excitation coils are placed in a small part of the transmitter coil. To induce voltage in the transmitter, the excitation coils need to generate magnetic fields that rotate along the cross-section of the transmitter coil as shown in Fig. 12(b).

Fig. 13 shows simulated self-inductances of the excitation coil (L_{ex}), transmitter coil (L_{tx}), and receiver coil (L_{rx}) with l_g. When the opening l_g is small, the rate of decrease of L_{ex} is very fast as the l_g increases. It is because total magnetic flux in the core is inversely proportional to the value of $l_g + l_f/\mu_r$ when the gap l_g is comparable to l_f/μ_r. If l_g is much bigger than l_f/μ_r, the flux is dependent only on l_g, and L_{ex} decreases slowly. It should be noted that the inductance L_{tx} also decreases as l_g increases. Since the ferrite core encircles the transmitter coil, the inductance of the transmitter coil is increased when the l_g is small. However, L_{tx} decreases as l_g and corresponding reluctance increase. As the excitation

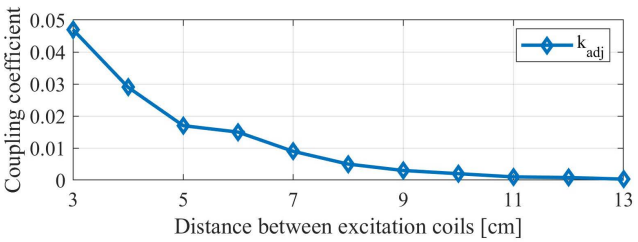

FIGURE 15. FEA results of coupling coefficient between adjacent excitation coils (N=4).

TABLE 2. Selected parameters of excitation coil.

Core material (PL11)			
l_f	26 cm	S	10 cm^2
μ_f	2500	B_{sat}(23°C)	510 mT
N_{ex}	7	l_g	1 mm

coils have very weak couplings with the receiver coil, L_{rx} is independent to the opening l_g.

Fig. 14(a) shows the mutual-inductance (M_{extx}) and the coupling coefficient (k_{extx}) between the excitation and transmitter coils with l_g. The leakage flux of excitation coils increases with an increase in l_g. Consequently, k_{extx} and the M_{extx} also decrease. To achieve a strong coupling between the excitation and transmitter coils, a smaller l_g is suitable. However, L_{ex} and L_{tx} are very sensitive to l_g when l_g is small as shown in Fig. 13. There is a trade-off relationship between the strong coupling k_{extx} and the parameter robustness of L_{ex} and L_{tx}. To enhance the parameter robustness of the excitation and transmitter coils, the air-gap length l_g is chosen to be 1 mm. Then, the number of turns, N_{ex}, is chosen to be 7 to achieve the target self-inductance of the excitation coil in TABLE 1 with l_g of 1 mm. Selected design results of the excitation coil are listed in TABLE 2.

Fig. 14(b) shows the mutual-inductance (M_{txrx}) and the coupling coefficient (k_{txrx}) between the transmitter and receiver coils with l_g. It should be noted that the M_{txrx} is irrelevant to the l_g. Because the k_{txrx} increases while the L_{tx} decreases depending on the length of the l_g.

In section II, the circuit analysis assumes that the excitation coils have no magnetic coupling with each other. Therefore, the cross-couplings between adjacent excitation coils with the selected design are investigated. k_{adj} is the coupling coefficient between adjacent excitation coils. Fig. 15 shows k_{adj} depending on the distance between excitation coils. It should be noted that the cross-couplings between adjacent excitation coils can be neglected when the distance between them is greater than 10 cm.

IV. EVALUATION OF PROPOSED MULTILEVEL IPT SYSTEM

To evaluate the proposed multilevel on-line IPT system, a four-level IPT system was built. The test setup has the same mechanical and electrical parameters as the simulation model in section III and Fig. 12. Litz-wires with 1000, 4000 and

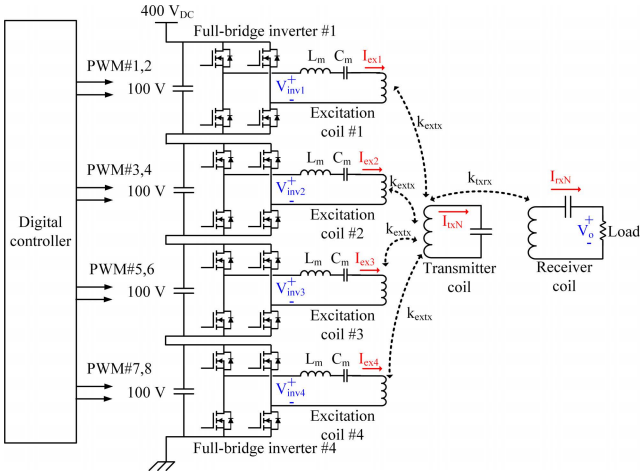

FIGURE 16. Configuration of the test-bed.

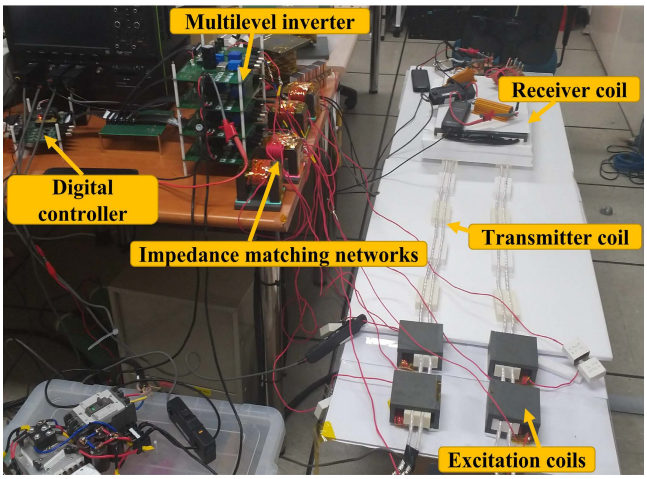

FIGURE 17. Photo of the four-level IPT system test-bed.

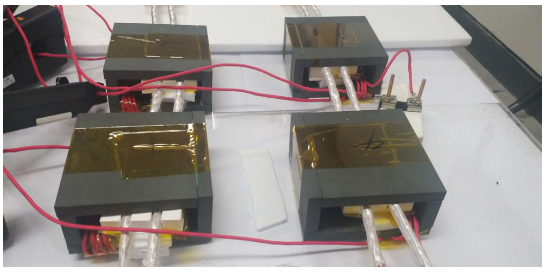

FIGURE 18. Photo of excitation coils of the four-level IPT system.

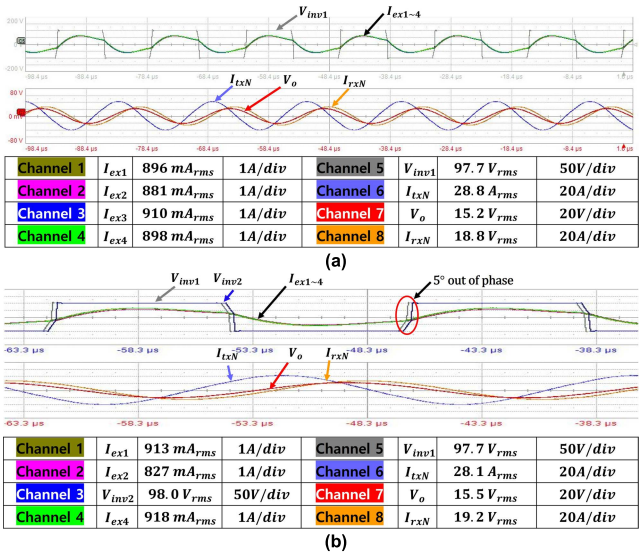

Channel 1	I_{ex1}	896 mA_{rms}	1A/div	Channel 5	V_{inv1}	97.7 V_{rms}	50V/div
Channel 2	I_{ex2}	881 mA_{rms}	1A/div	Channel 6	I_{txN}	28.8 A_{rms}	20A/div
Channel 3	I_{ex3}	910 mA_{rms}	1A/div	Channel 7	V_o	15.2 V_{rms}	20V/div
Channel 4	I_{ex4}	898 mA_{rms}	1A/div	Channel 8	I_{rxN}	18.8 V_{rms}	20A/div

(a)

Channel 1	I_{ex1}	913 mA_{rms}	1A/div	Channel 5	V_{inv1}	97.7 V_{rms}	50V/div
Channel 2	I_{ex2}	827 mA_{rms}	1A/div	Channel 6	I_{txN}	28.1 A_{rms}	20A/div
Channel 3	V_{inv2}	98.0 V_{rms}	50V/div	Channel 7	V_o	15.5 V_{rms}	20V/div
Channel 4	I_{ex4}	918 mA_{rms}	1A/div	Channel 8	I_{rxN}	19.2 V_{rms}	20A/div

(b)

FIGURE 19. Experimental waveforms. (a) Case 1: when four inverter's output voltage sources are in-phase. b) Case 2: when one inverter's output voltage source is out-of-phase.

2000 strands were used for the excitation, transmitter and receiver coils, respectively. The strand diameter was chosen to be 120 μm. Figs. 16 and 17 show a configuration and a photo of the setup. Fig. 18 shows a photo of the designed excitation coils. The target IPT system consists of four series-connected full-bridge inverters, four excitation coils, a transmitter coil, a receiver coil (air-gap 7 cm between the transmitter and the receiver), and a load resistor. The input voltages of the inverters were regulated at 100 V. Four SiC MOSFETs (C3M0120090D, Cree/Wolfspeed [19]) were used for the full-bridge inverters. The switching frequency of the inverters was 64 kHz which was the tuned frequency of the receiver coil. The circuit parameters of the setup are same as the parameters in TABLE 1.

Fig. 19 presents measured voltage and current waveforms for two different operations: 1) when the four inverters' output voltages are in-phase and 2) when an output voltage of the inverters is out-of-phase with the others. Fig. 19(a) shows measured voltage and current waveforms of the inverter, excitation, transmitter, and receiver coils when the inverter output voltages are in-phase. It should be noted that all excitation coil currents had nearly the same magnitudes and phases and the input impedances were well balanced, which makes it easy to balance the cell voltages of the multilevel system. Each inverter delivered the same output power of 68.5 W to the load, and the total output power was 273 W. The average of the root-mean-square (rms) values of the four excitation coil currents were 894 mA_{rms}, while the rms of the transmitter was 28.8 A_{rms}. Therefore, the current gain from the excitation coil current to the transmitter coil current was 32, and it agreed very well with the theoretical result in Fig. 8(a). At this operating condition, the sum of the input powers of the four coils was 310 W, and the measured power from the 400 V DC power supply was 325 W. Therefore, coil-to-coil efficiency was 88%, and DC-to-load efficiency was 84% over the 7 cm air-gap.

Fig. 19(b) shows the voltages and currents of the system when there is 5° phase mismatch between the inverters. It should be noted that the excitation coil currents were synchronized even if their voltages had 5° phase mismatch, as shown in the first grid. The magnitude of the mismatched inverter's current I_{ex2} decreased from 881 to 827 mA_{rms} and the other excitation coil currents increased about 2%. Therefore, the small mismatch of the inverter's output voltage

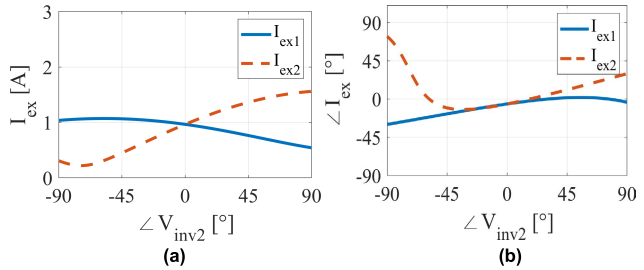

FIGURE 20. Excitation coil currents as one of inverter voltage is out of phage. (a) Magnitude of excitation coil currents. (b) Phase of excitation coil currents.

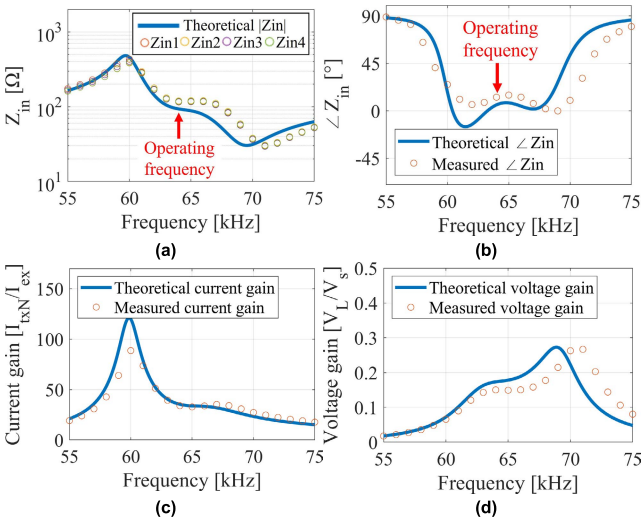

FIGURE 21. Theoretical and experimental frequency responses. (a) Magnitudes of input impedance. (b) Phases of input impedance. (c) Current gain of the transmitter coil current to the excitation coil current. (d) Voltage gain of the load voltage to the dc voltage.

has a negligible impact on the transmitter coil current and corresponding output voltage of the receiver coil. To verify the measured result, the dependence of the currents of the excitation coils on the phase mismatch of the inverter voltages are calculated using the equivalent circuit in Fig 4. Fig. 20 shows the calculated magnitude and phase of the excitation coils on the phase mismatch of V_{inv2}. In this figure, I_{ex1} is the current of the excitation coil connected to the inverter that is synchronized with the other inverters, and I_{ex2} is the current of the excitation coil connected to the inverter that is out-of-phase. In Fig. 20(a), it should be noted that the magnitude of I_{ex2} is reduced 5% while the magnitudes of the other excitation coil currents are increased 2% when the phase of V_{inv2} is $-5°$. This result agrees very well with the measured result. Furthermore, the excitation coil currents have the same phases when the phase mismatch is in the range of $-45°$ to $+10°$ as shown in Fig. 20(b). This theoretical analysis explains the experimental result in Fig. 19(b). This result shows the robustness of the proposed multilevel IPT system on phase mismatches between the inverters.

Fig. 21 shows the theoretical and measured frequency responses of the proposed IPT system. The theoretical and measured input impedances seen from the four inverters are shown in Fig. 21(a) and (b). The current gain of the transmitter coil to the excitation coil and the voltage gain of the load to the source voltage of the inverters are shown in Fig. 21(c) and (d). This result shows the validity of the circuit analysis in section II.

V. CONCLUSION

A novel transformerless multilevel on-line IPT system is proposed in this study. The proposed system utilizes multiple excitation coils with strong magnetic couplings to a transmitter coil. It was found that the voltages induced by multiple excitation coils can be augmented on the transmitter coil because all excitation coil currents have the same frequency and phase. The excitation coils significantly help in improving modularization, fail-safe operation, power density, providing galvanic isolation, and ensuring high electrical insulation. Equivalent circuit models were developed to analyze the proposed multilevel IPT system. An example 4-level IPT system was designed to evaluate the proposed topology.

Using simulation results, the magnetic couplings between the excitation, transmitter, and receiver coils, depending on

$$
\begin{aligned}
f_{r3} &= \frac{1}{2\pi}\sqrt{\left|\frac{-b-d-e}{3a}\right|} \; for\; N \geq 2 \\
a &= \frac{-1+k_{txrx}^2+k_{extx}^2 L_{ex} C_m \omega_{r1}^2 N}{\omega_{r1}^2 \omega_{tx}^2 \omega_{rx}^2} \\
b &= \frac{\omega_{tx}^2+\omega_{rx}^2+\omega_{r1}^2-k_{txrx}^2\omega_{r1}^2-k_{extx}^2 L_{ex} C_m \omega_{r1}^2 \omega_{rx}^2 N}{\omega_{r1}^2 \omega_{tx}^2 \omega_{rx}^2} \\
c &= -\frac{1}{\omega_{r1}^2}-\frac{1}{\omega_{tx}^2}-\frac{1}{\omega_{rx}^2} \\
d &= \sqrt[3]{\frac{1}{2}[2b^3-9abc+27a^2+\sqrt{(2b^3-9abc+27a^2)^2-4(b^2-3ac)^3}]} \\
e &= \sqrt[3]{\frac{1}{2}[2b^3-9abc+27a^2-\sqrt{(2b^3-9abc+27a^2)^2-4(b^2-3ac)^3}]}
\end{aligned} \tag{10}
$$

the shape of the excitation coils were investigated. The self-inductance of the transmitter coil is influenced by the shape of the excitation coils, but the mutual-inductance between the transmitter coil and the receiver coil is not. The designed shape of the excitation coil is based on a trade-off relationship between the strong coupling between the excitation and transmitter coils and the parameter robustness of the self-inductances of the excitation and transmitter coils.

The viability of the proposed IPT system was evaluated using the experimental results. The experimental results were in good agreement with the theoretical results. Measured coil-to-coil and DC-to-load efficiencies of the proposed system were 88% and 84%, respectively, over the 7 cm air-gap.

Appendix

The closed solution of the third resonant frequency f_{r3} follows (10), as shown at the bottom of the previous page.

REFERENCES

[1] S. Zhou, X. Wang, Y. Sun, J. Zhu, J. Tan, and Z. Zuo, "Single-source cascaded multilevel inverter for magnetic coupling wireless power transfer systems," in *Proc. IMCEC*, Chongqing, China, Oct. 2019, pp. 910–915, doi: 10.1109/IMCEC46724.2019.8983927.

[2] L. Yang, X. Li, S. Liu, Z. Xu, C. Cai, and P. Guo, "Analysis and design of three-coil structure WPT system with constant output current and voltage for battery charging applications," *IEEE Access*, vol. 7, pp. 87334–87344, 2019, doi: 10.1109/ACCESS.2019.2925388.

[3] M. Kiani and M. Ghovanloo, "The circuit theory behind coupled-mode magnetic resonance-based wireless power transmission," *IEEE Trans. Circuits Syst. I, Reg. Papers*, vol. 59, no. 9, pp. 2065–2074, Sep. 2012, doi: 10.1109/TCSI.2011.2180446.

[4] H. Hao, G. A. Covic, and J. T. Boys, "A parallel topology for inductive power transfer power supplies," *IEEE Trans. Power Electron.*, vol. 29, no. 3, pp. 1140–1151, May 2014, doi: 10.1109/TPEL.2013.2262714.

[5] D. Patil, M. K. McDonough, J. M. Miller, B. Fahimi, and P. T. Balsara, "Wireless power transfer for vehicular applications: Overview and challenges," *IEEE Trans. Transport. Electrific.*, vol. 4, no. 1, pp. 3–37, Mar. 2018, doi: 10.1109/TTE.2017.2780627.

[6] A. El-Shahat, E. Ayisire, Y. Wu, M. Rahman, and D. Nelms, "Electric vehicles wireless power transfer state-of-the-art," *Energy Proc.*, vol. 162, pp. 24–37, Apr. 2019, doi: 10.1016/j.egypro.2019.04.004.

[7] A. Zaheer, G. A. Covic, and D. Kacprzak, "A bipolar pad in a 10-kHz 300-W distributed IPT system for AGV applications," *IEEE Trans. Ind. Electron.*, vol. 61, no. 7, pp. 3288–3301, Jul. 2014, doi: 10.1109/TIE.2013.2281167.

[8] J. Huh, S. W. Lee, W. Y. Lee, G. H. Cho, and C. T. Rim, "Narrow-width inductive power transfer system for online electrical vehicles," *IEEE Trans. Power Electron.*, vol. 26, no. 12, pp. 3666–3679, Dec. 2011, doi: 10.1109/TPEL.2011.2160972.

[9] J. H. Kim, B.-S. Lee, J.-H. Lee, S.-H. Lee, C.-B. Park, S.-M. Jung, S.-G. Lee, K.-P. Yi, and J. Baek, "Development of 1-MW inductive power transfer system for a high-speed train," *IEEE Trans. Ind. Electron.*, vol. 62, no. 10, pp. 6242–6250, Oct. 2015, doi: 10.1109/TIE.2015.2417122.

[10] Y. Li, R. Mai, M. Yang, and Z. He, "Cascaded multi-level inverter based IPT systems for high power applications," *J. Power Electron.*, vol. 15, no. 6, pp. 1508–1516, Nov. 2015, doi: 10.6113/JPE.2015.15.6.1508.

[11] S.-J. Park, F.-S. Kang, S. E. Cho, C.-J. Moon, and H.-K. Nam, "A novel switching strategy for improving modularity and manufacturability of cascaded-transformer-based multilevel inverters," *Electr. Power Syst. Res.*, vol. 74, no. 3, pp. 409–416, Jun. 2005, doi: 10.1016/j.epsr.2005.01.005.

[12] R. Ayyanar, R. Giri, and N. Mohan, "Active input-voltage and load-current sharing in input-series and output-parallel connected modular DC-DC converters using dynamic input-voltage reference scheme," *IEEE Trans. Power Electron.*, vol. 19, no. 6, pp. 1462–1473, Nov. 2004, doi: 10.1109/TPEL.2004.836671.

[13] C. Gu, Z. Zheng, Y. Li, H. Ma, and Z. Gao, "Power balancing control of a multilevel converter using high-frequency multi-winding transformer," in *Proc. IPEMC*, Harbin, China, Jun. 2012, pp. 1866–1870, doi: 10.1109/IPEMC.2012.6259122.

[14] E. S. Deepak, C. S. Anil, S. Sanjay, C. Febi, and K. R. Sajina, "A novel multilevel inverter topology based on multi-winding multi-tapped transformers for improved wave shape requirements," in *Proc. IICPE*, New Delhi, India, Jan. 2011, pp. 1–5, doi: 10.1109/IICPE.2011.5728136.

[15] A. K. Sahoo and N. Mohan, "High frequency link multi-winding power electronic transformer using modular multilevel converter for renewable energy integration," in *Proc. IECON*, Dallas, TX, USA, Oct. 2014, pp. 4642–4648, doi: 10.1109/IECON.2014.7049202.

[16] J. Lee, M.-Y. Kim, and S.-H. Lee, "A new multilevel inductive power transfer system," in *Proc. WoW*, Seoul, South Korea, Nov. 2020, pp. 264–270, doi: 10.1109/WoW47795.2020.9291259.

[17] Samwha Electronics, Yongin-si, South Korea. *PL11*. Accessed: Jan. 1, 2021. [Online]. Available: http://www.samwha.co.kr/electronics/

[18] ANSYS, Canonsburg, PA, USA. (2019). *HFSS 20*. Accessed: Mar. 8, 2021. [Online]. Available: https://www.ansys.com/

[19] Wolfspeed, Research Triangle Park, NC, USA. *C3M0120090D*. Accessed: May 4, 2021. [Online]. Available: https://www.wolfspeed.com/power/products/sic-mosfets/

JAEHONG LEE (Graduate Student Member, IEEE) received the B.S. degree in electrical engineering from the University of Seoul, Seoul, South Korea, in 2019, where he is currently pursuing the Ph.D. degree in electrical engineering. His current research interests include wireless power transfer systems and solid state transformers.

MYUNG-YONG KIM (Member, IEEE) received the B.S. and M.S. degrees in electrical engineering from Chung-Ang University, Seoul, South Korea, in 1989 and 1991, respectively. From 1991 to 1995, he was a Senior Researcher with the Traction Research Group, Hyundai Precision and Industries Company, South Korea. Since 1995, he has been working with the Korea Railroad Research Institute, Uiwang, South Korea, where he is currently a Principal Researcher. His research interests include wireless power transfer systems and power converter systems especially for railway vehicles.

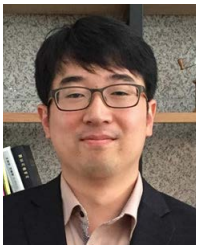

SEUNG-HWAN LEE (Member, IEEE) received the B.S. degree (Hons.) in mechanical engineering and electrical engineering and the M.S. degree in electrical engineering from Seoul National University, Seoul, South Korea, in 2004 and 2008, respectively, and the Ph.D. degree in mechanical engineering from the University of Wisconsin–Madison (WEMPEC), Madison, WI, USA, in 2013. He was a Senior Researcher at the Korea Railroad Research Institute (KRRI). He is currently an Associated Professor at the University of Seoul, Seoul. His current research interests include the power electronics, resonant wireless power transfer systems, resonant power converter, high frequency magnetic components design, and intelligent power electronics transformers.